Supporting Information

Inverse analysis-guided development of acid-tolerant nanoporous high-entropy alloy catalysts for enhanced water-splitting performance

Saikat Bolar,[a] *Chunyu Yuan,*[a] *Samuel Jeong*,[b] *Yoshikazu Ito*[b] *and Takeshi Fujita* *[a]

[a] School of Engineering Science, Kochi University of Technology, 185 Miyanokuchi, Tosayamada, Kami City, Kochi 782-8502, Japan

[b] Institute of Applied Physics, Graduate School of Pure and Applied Sciences, University of Tsukuba, Tsukuba 305-8573, Japan

*E-mail: fujita.takeshi@kochi-tech.ac.jp

Experimental procedures for membrane electrode assembly

1. 1 Preparation of catalyst inks and fabrication of membrane electrode assembly for Pt/C||IrO_2

A 1.0 cm^2 Pt/C||IrO_2 membrane electrode assembly was prepared using a conventional spray-coating method. A homogeneous ink for the cathode catalyst layer was prepared from Pt/C (10 mg), Nafion™ solution (54 μL), and isopropyl alcohol/water solution (1.8:0.2 mL). The ink was sonicated for 10 min and then spray-coated onto a preheated (120 °C) Nafion®117 membrane (front side; area: 1.0 cm^2) to form the cathode catalyst layer (catalyst loading: 1.0 mg cm^{-2}). Next, a homogeneous ink for the anode catalyst layer was prepared from IrO_2 (10 mg), Nafion™ solution (25 μL), and isopropyl alcohol/water solution (1.5:1.5 mL). The ink was sonicated for 30 min and then spray-coated onto the preheated (120 °C) Nafion®117 membrane (back side) to form the anode catalyst layer (catalyst loading: 1.0 mg cm^{-2}). Finally, a 1.0 cm^2 piece of carbon paper (GDL 22 BB, SIGRACET) was hot-pressed onto the cathode catalyst layer at 130 °C and 5.0 MPa for 1 min to form the cathode gas diffusion layer.

1.2 Preparation of catalyst inks and fabrication of membrane electrode assembly for HEA8||IrO_2

A 1.0 cm^2 HEA8||IrO_2 membrane electrode assembly was prepared using a similar spray-coating method. The homogeneous ink for the cathode catalyst layer comprised as-synthesized HEA8 (20 mg), Nafion™ solution (40 μL), and isopropyl alcohol/water solution (1:1 mL). The ink was sonicated for 30 min and then spray-coated onto a preheated (120 °C) Nafion®117 membrane (front side; area: 1.0 cm^2) to form the cathode catalyst layer (catalyst loading: 0.85 mg cm^{-2}) (Pt base). The homogeneous ink for the anode catalyst layer was the same as that for the Pt/C||IrO_2 assembly. The ink was sonicated for 30 min and then spray-deposited onto the preheated (120 °C) Nafion®117 membrane (back side) to form the anode catalyst layer (catalyst loading: 1.5 mg cm^{-2}). Finally, 1.0 cm^2 piece of carbon paper was hot-pressed onto the cathode catalyst layer at 130 °C and 5.0 MPa for 1 min to form the cathode gas diffusion layer.

1.3 Preparation of catalyst inks and fabrication of membrane electrode assembly for Pt/C||HEA8

A 1.0 cm^2 Pt/C||HEA8 membrane electrode assembly was prepared using a similar spray-coating method. A homogeneous Pt/C ink was prepared as for the Pt/C||IrO_2 assembly and then spray-coated onto a preheated (120 °C) Nafion®117 membrane (front side; area: 1.0 cm^2) to form the cathode catalyst layer (catalyst loading: 1.0 mg cm^{-2}). A homogeneous ink for the anode catalyst layer was prepared from as-synthesized HEA8 (20 mg), Nafion™ solution (40 μL), and isopropyl alcohol/water solution (1:1 mL). The ink was sonicated for 30 min and then spray-coated onto a preheated (120 °C) Pt-plated Ti mesh (i.e., porous transport layer) to form the anode catalyst layer (catalyst loading: 0.85 mg cm^{-2}) (Pt base). A 1.0 cm^2 piece of carbon paper was hot-pressed onto the cathode catalyst layer on the Nafion®117 membrane at 130 °C and 5.0 MPa for 1 min to form the cathode gas diffusion layer. Subsequently, the porous transport layer was joined with the membrane in the cell.

1.4 Electrolyzer cell setup

A standard electrolyzer cell (YNU standard cell) was employed for the proton exchange membrane (PEM) test. The membrane electrode assembly (gas diffusion layer + Nafion®117) was placed between the flow fields with a porous transport layer on the anode. Two gaskets (thickness: 160 μm each) were placed on the anode side and one gasket (thickness: 160 μm) was placed on the cathode side for sealing and insulation. The membrane electrode assembly was then pressed at 3 MPa.

1.5 Cell testing

Single-cell tests were performed using a potentiostat (VSP-300, Biologic) equipped with a booster unit (10 A). All measurements were performed at a cell temperature of 80 °C under ambient pressure. Deionized water (18.2 MΩ cm, Millipore) was preheated at 90 °C and fed to the anode side of the cell at a water flow rate of 10 mL min^{-1}. After the cell temperature was stabilized at 80 °C, the cell was conditioned by ramping the

current density to 3.0 A cm^{-2} and holding the current density for 3 h for cell activation. Subsequently, stable current–voltage (*I–V*) polarization curves were recorded from 0 to 5.0 A cm^{-2} at a scan rate of 10 mV s^{-1}. Chronoamperometry was performed for 100 h at a cell voltage of 1.57 V for HEA||IrO_2, 1.70 V for Pt/C||HEA8, and 1.65 V for Pt/C||IrO_2.

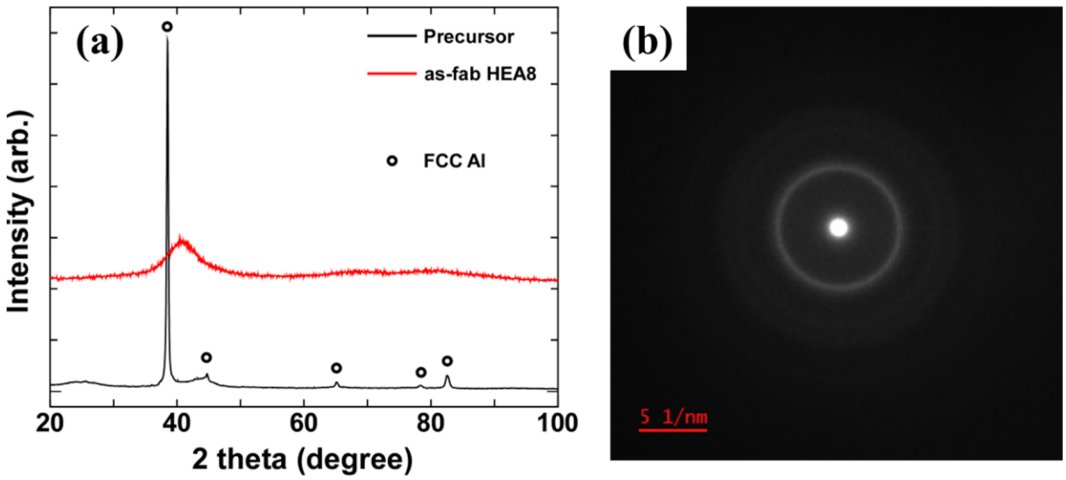

Figure S1. (a) XRD patterns of the as-fabricated HEA8 alloy and as-prepared Al-alloy precursor ribbons. (b) Selected area electron diffraction pattern of HEA8.

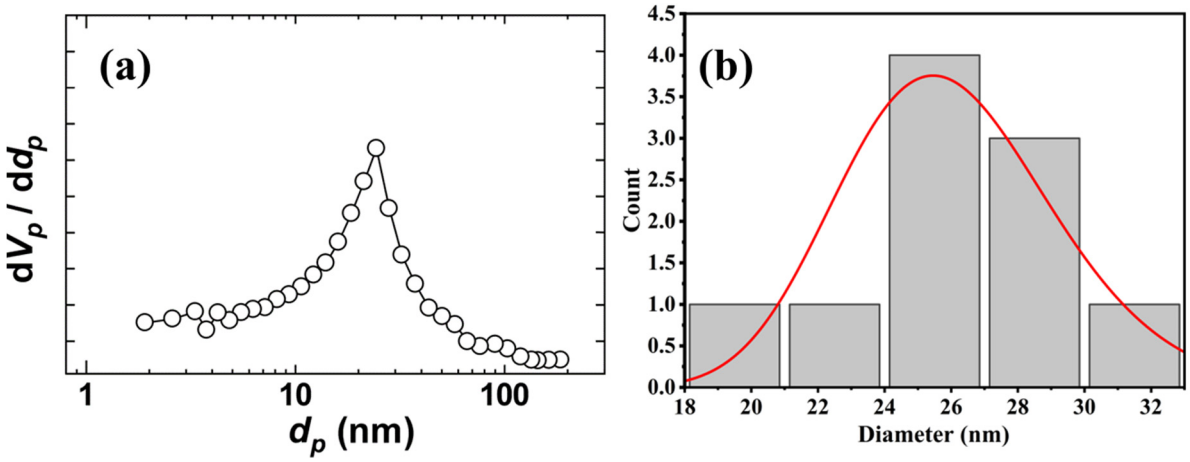

Figure S2. (a) Barrett–Joyner–Halenda (BJH) pore size distribution of HEA8, displaying hierarchical distribution with a broad peak corresponding to pores in the range of ~20–30 nm. (b) Particle diameter histogram obtained from TEM observations (Figure S3a), showing consistency with the BJH pore size distribution.

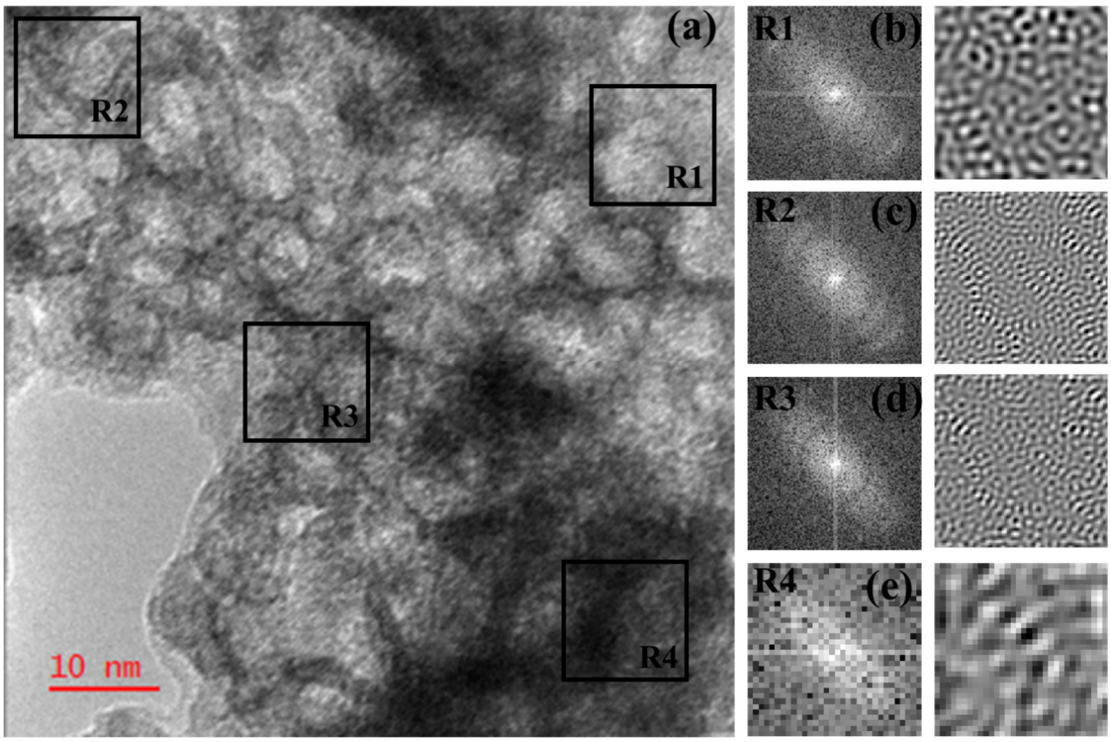

Figure S3. (a) TEM image of HEA8 and (b–e) fast Fourier transform and inverse fast Fourier transform patterns at different regions (R1–R4). The broadened and diffuse spots indicate nonuniform atomic positions and distorted lattice planes.

Table S1. ICP analysis of HEA8, with the sum of the analyzed elements set to 100%.

Element	**Atomic percent (%)**
Al	27.7
Pt	13.3
Rh	12.3
Ir	13.5
Au	14.7
Ru	13.2
Nb	2.6
Ta	2.6

Table S2. Recently reported electrocatalysts for the hydrogen evolution reaction (HER) in acidic media.

Electrocatalyst	Overpotential (η_{10})	Tafel Slope (mV dec^{-1})	Ref.
$Mo_{0.58}V_{0.26}Nb_{0.16}Se_2$	80	55	1
$Nb_{0.7}V_{0.3}Se_2$	236	72	2
PtFeCoNiCuHEA	10.8	28.1	3
PtSA/NT/NF	24	30	4
ALDPt/NGNs	48	29	5
$Mo_2TiC_2T_x$-PtSA	30	30	6
Pt/np-$Co_{0.85}Se$	55	35	7
PbPtCuNiP	62	44.6	8
K_2PtCl_4/NC	11	21	9
Pt/MC	27.3	26	10
AL-Pt/Pd_3Pb	13.8	18	11
M-$CoSe_{1.28}S_{0.72}$	67	50	12
HEA8	41	87.2	This work

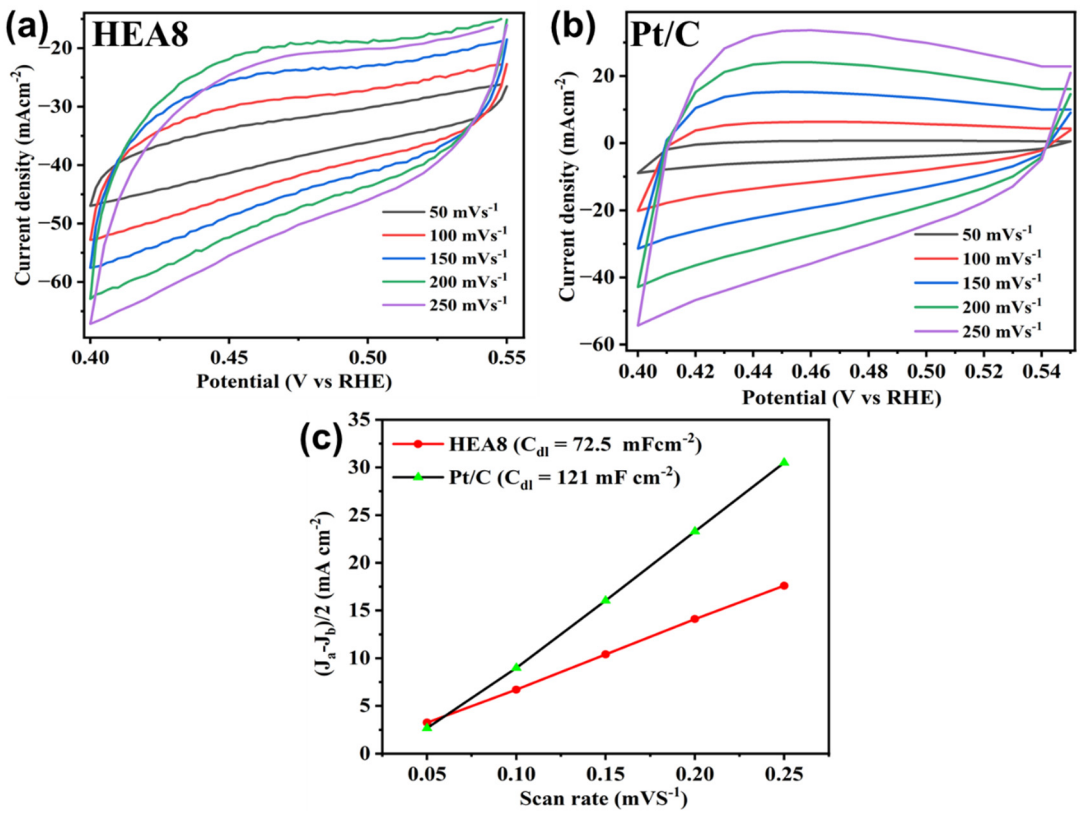

Figure S4. Cyclic voltammograms and electrochemically active surface areas (ESCAs) of HEA8 and Pt/C for the HER.

Table S3. Tafel slope (*b*), intercept (*a*), and exchange current density (j_0) related to the HER catalyzed by different materials.

Electrocatalyst	Steady-state region		
	a	***b* (mV dec^{-1})**	**j_0 (mA cm^{-2})**
HEA8	−0.05548	87.2	4.16
Pt/C	−0.01131	67.5	1.69

Table S4. Calculated double-layer capacitance (C_{dl}), ECSA, and roughness factor (RF).

Catalyst	C_{dl} (mFcm^{-2})	ECSA (cm^2)	RF
HEA8	78.5	2242.28	56057
Pt/C	121	3457.14	86425

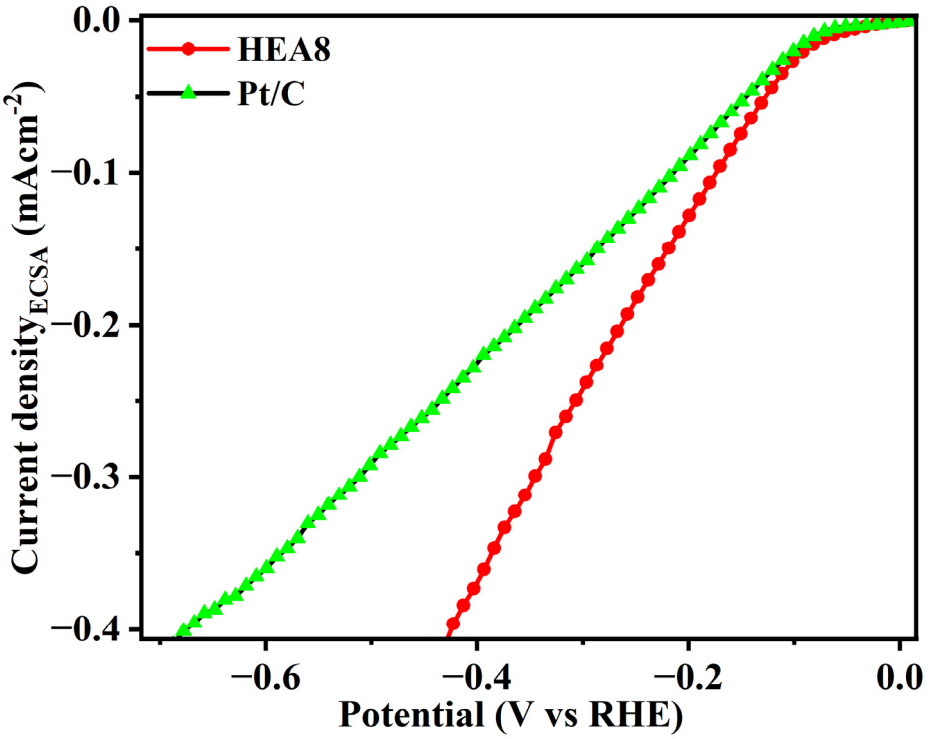

Figure S5. ECSA-normalized linear sweep voltammograms of HEA8 and Pt/C.

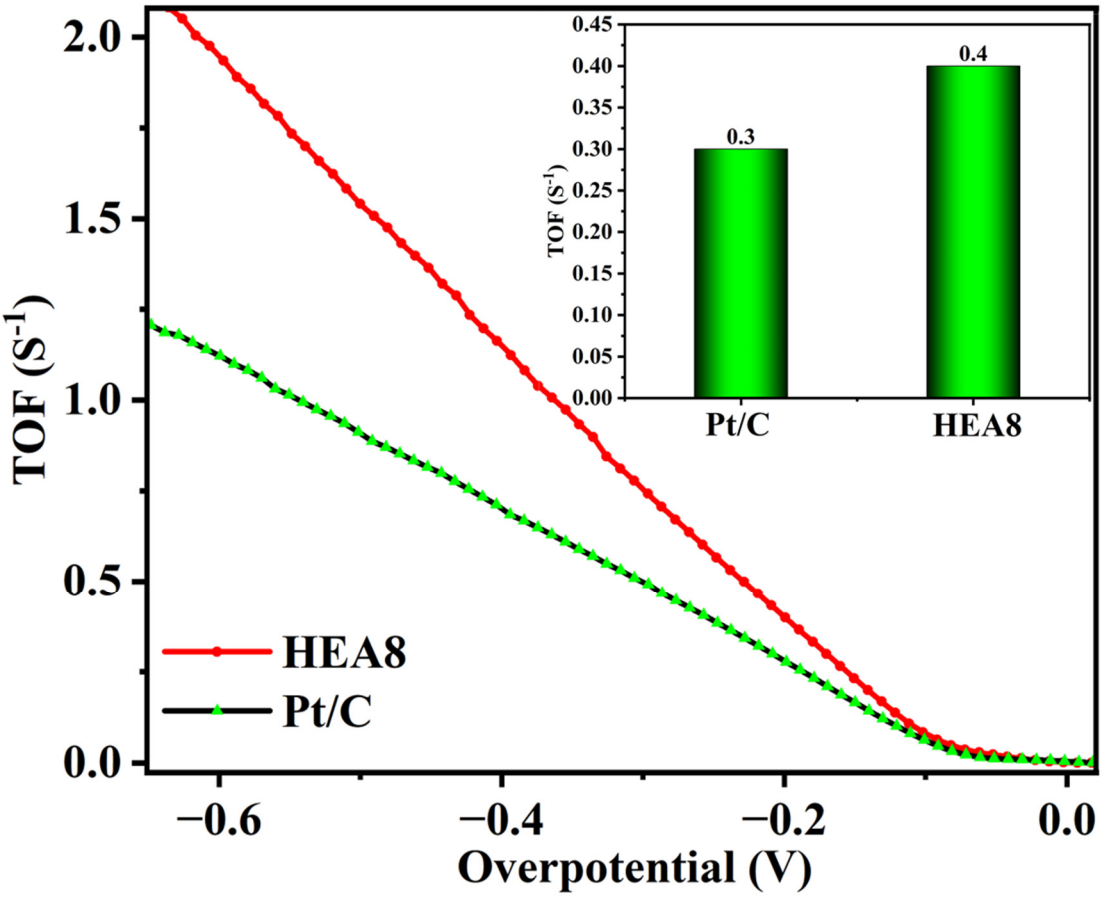

Figure S6. Turnover frequencies (TOFs) for the investigated HER electrocatalysts (inset: comparison of TOFs for HEA8 and Pt/C at an overpotential of 200 mV).

TOF calculation for the HER

The method proposed by Jaramillo et al. was adopted for calculating the TOF.[13,14] The TOF was determined using the following equation:

$$\text{TOF per site} = \# \times J \times A/N \times A$$

where # represents the number of hydrogen turnover events, J is the current density at an applied overpotential, A is the geometric area of the catalyst, and N is the number of active sites per unit area. The total number of hydrogens turnovers ($\#H_2$) was calculated from the current density:

$$\#H_2 = (j \text{ mA cm}^{-2}) \times (1 \text{ C s}^{-1}/1000 \text{ mA}) \times (1 \text{ mol e}^{-1}/96485 \text{ C}) \times (1 \text{ mol } H_2/2 \text{ mol e}^{-1}) \times (6.023 \times 10^{23} \text{ molecules } H_2/1 \text{ mol } H_2) = 3.12 \times 10^{15} \text{ } H_2 \text{ s}^{-1} \text{ cm}^{-2} \text{ per mA cm}^{-2}$$

In this work, # is 3.12×10^{15} s^{-1} cm^{-2} per mA cm^{-2}, and A is 0.04 cm^2, corresponding to the geometric area of the catalyst. The surface site density of all materials is reasonably approximated to be 10^{15} cm^{-2}. Therefore, N can be calculated through the formula N =

$C_{dl}/C_s \times 10^{15}$ cm^{-2}, where C_{dl} and C_s represent the double-layer and specific capacitance, respectively. For this calculation, a general C_s value of 0.035 mF cm^{-2} was used.

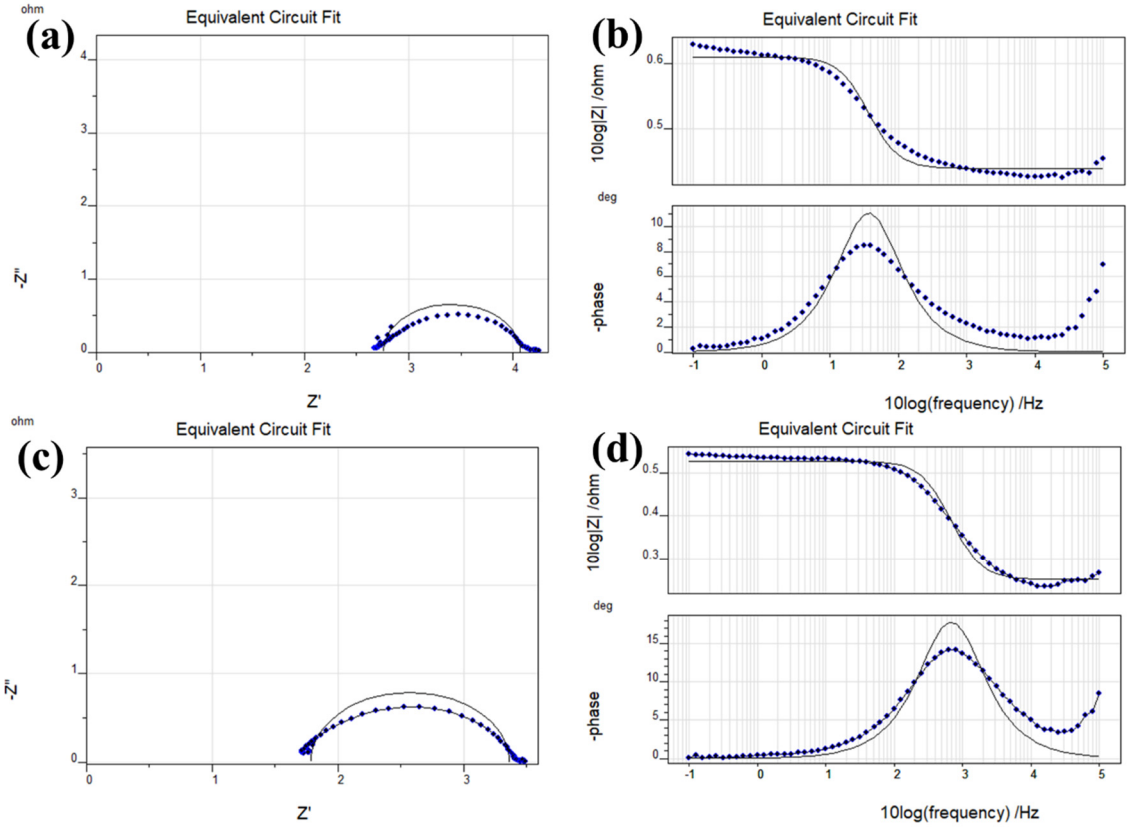

Figure S7. *Z*-fitting results with the equivalent circuit and Bode impedance plots for (a, b) HEA8 and (c, d) Pt/C.

Table S5. Fitted data from the Nyquist plots at an overpotential of 300 mV.

Catalyst	R_1 **(Ω)**	R_2 **(Ω)**	C_1 **(F)**
HEA8	2.757	1.312	0.00398
Pt/C	1.786	1.578	0.0002022

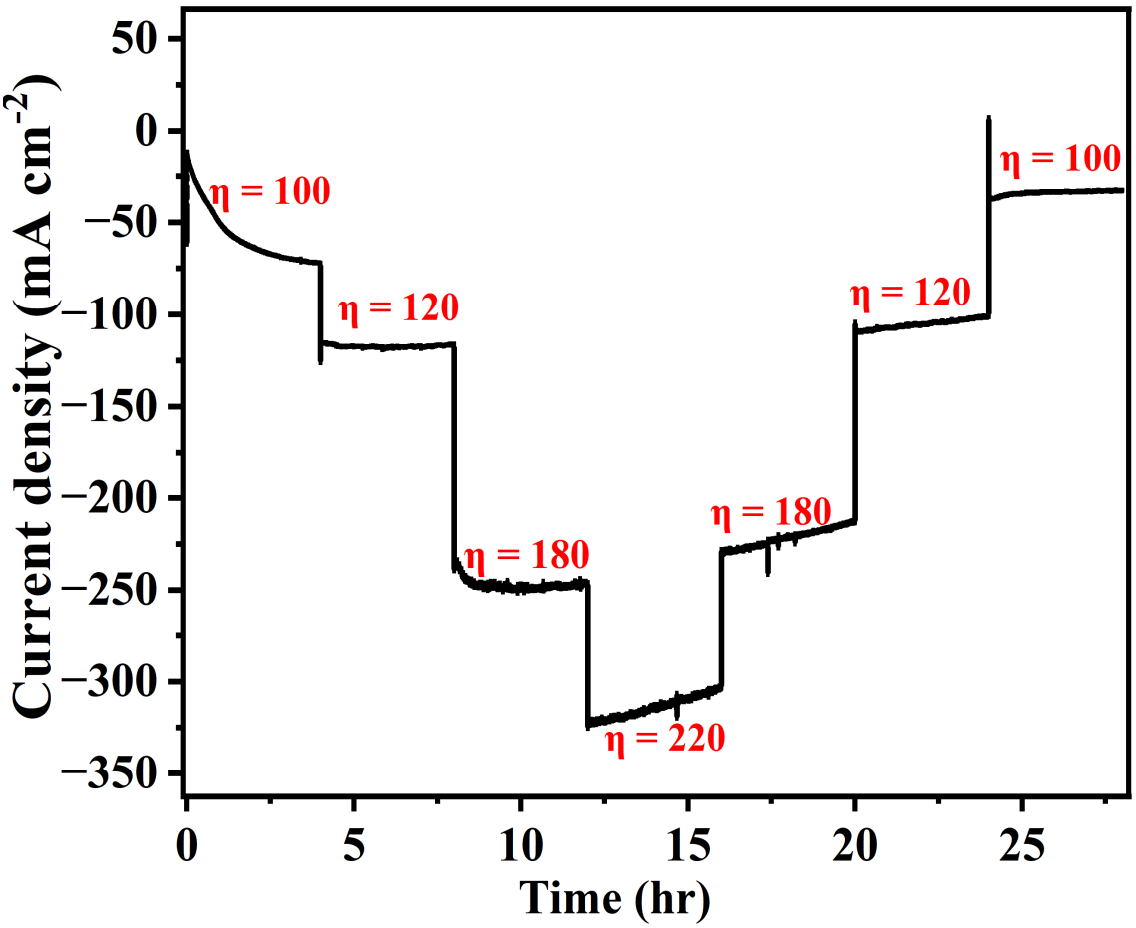

Figure S8. Chronoamperometry study of HEA8 at different potentials during the HER.

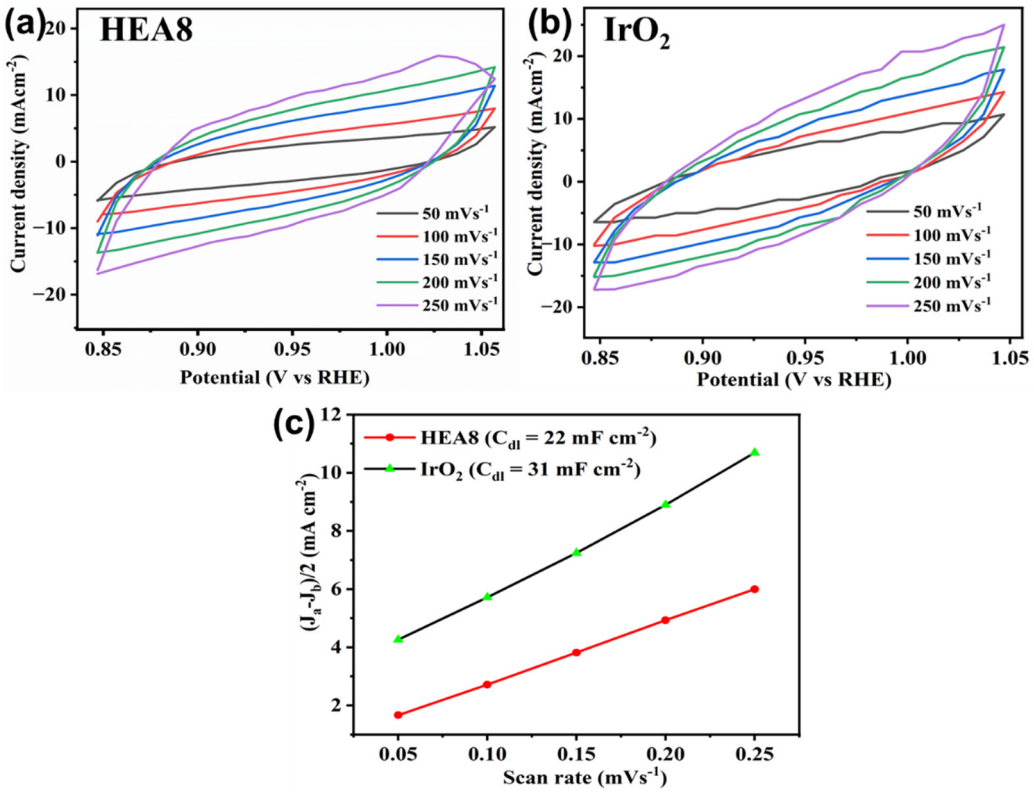

Figure S9. Cyclic voltammograms and ECSA of HEA8 and IrO_2 for the oxygen evolution reaction (OER).

Table S6. Tafel slope (*b*), intercept (*a*), and exchange current density (j_0) related to the OER catalyzed by different materials.

Electrocatalyst	**Steady-state region**		
	a	***b* (mV dec^{-1})**	**j_0 (mA cm^{-2})**
HEA8	0.084	89.2	0.199
IrO_2	0.130	52.7	0.063

Table S7. Calculated double-layer capacitance (C_{dl}), ECSA, and roughness factor (RF).

Catalyst	**C_{dl} (mF cm^{-2})**	**ECSA (cm^2)**	**RF**
HEA8	22	628.57	15714.25
IrO_2	31	885.71	22142.75

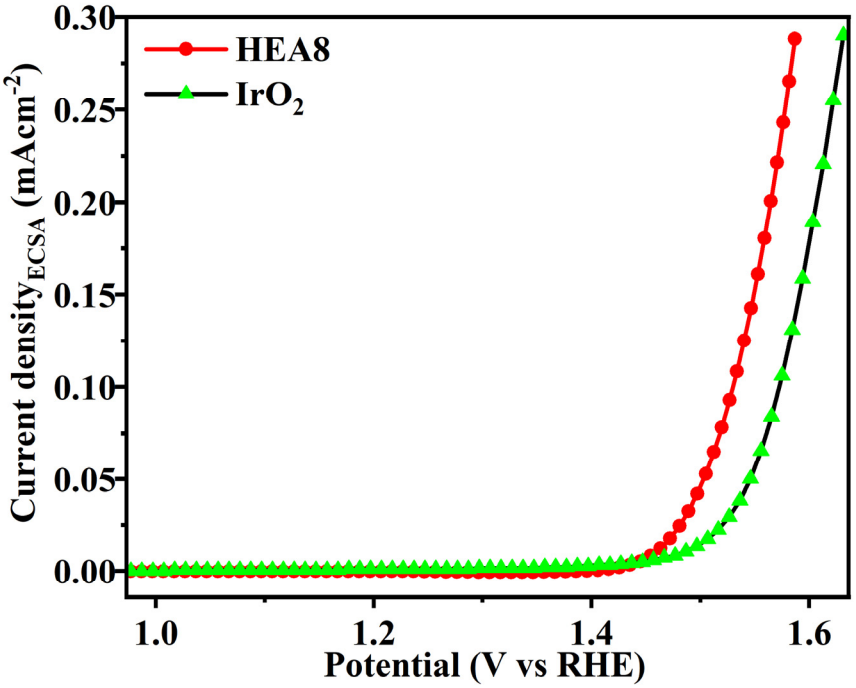

Figure S10. ECSA-normalized linear sweep voltammograms of HEA8 and IrO_2.

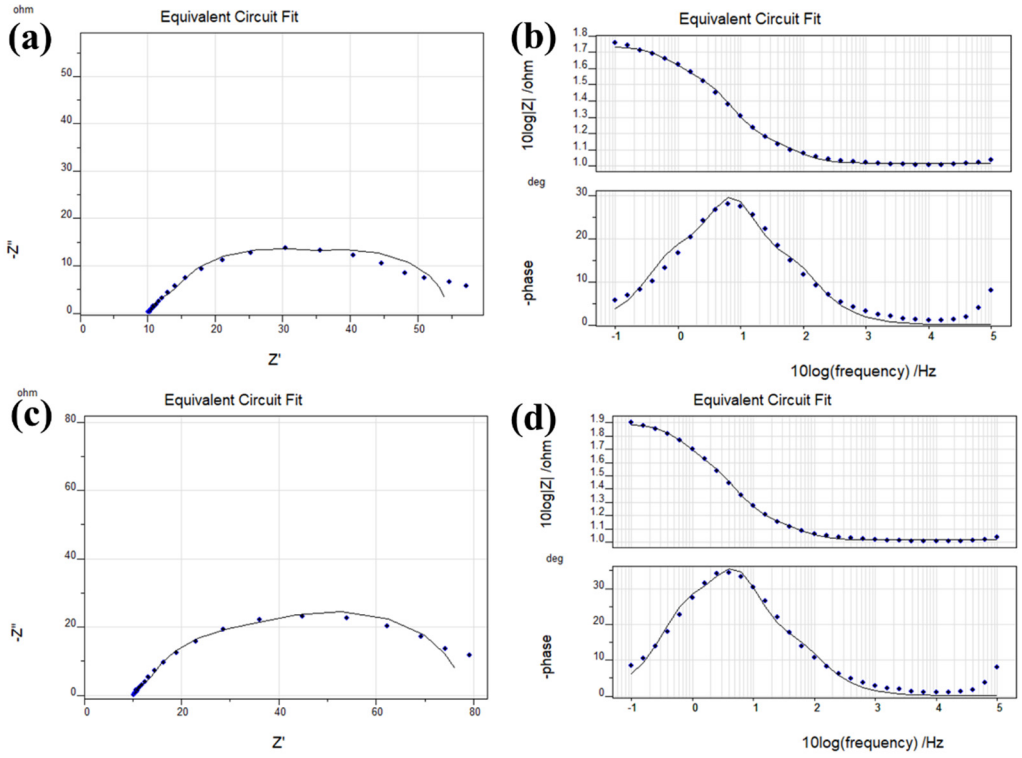

Figure S11. *Z*-fitting results with the equivalent circuit and Bode impedance plots for (a, b) HEA8 and (c, d) IrO_2.

Table S8. Fitted data from the Nyquist plots at an overpotential of 300 mV.

Catalyst	R_1 (Ω)	R_2 (Ω)	R_3 (Ω)	C_1 (F)	C_2 (F)
HEA8	10.24	0.001290	49.31	0.001299	0.000000009023
IrO_2	9.93	1.15	75.40	0.001730	0.0000001236

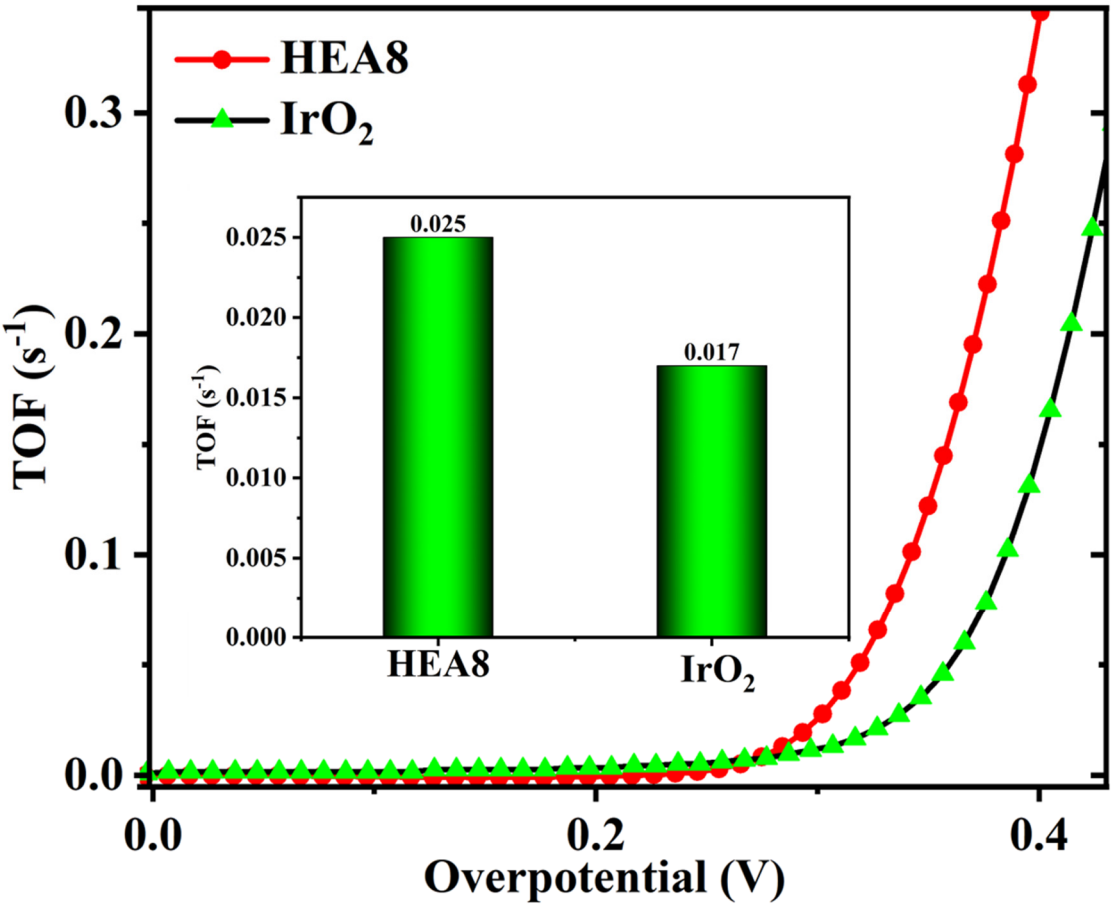

Figure S12. TOFs for the OER electrocatalysts (inset: comparison of TOFs for HEA8 and IrO_2 at an overpotential of 300 mV).

TOF calculation for the OER

The method proposed by Jaramillo et al. was adopted for calculating the TOF.[13,14] The TOF was determined using the following equation:

$$\text{TOF per site} = \# \times J \times A/N \times A$$

where # represents the number of hydrogen turnover events, J is the current density at an applied overpotential, A is the geometric area of the catalyst, and N is the number of active

sites per unit area. The total number of oxygen turnovers (#O_2) was calculated from the current density using the following equation:

#O_2 = (j mA cm^{-2}) × (1 C s^{-1}/1000 mA) × (1 mol e^{-1}/96485 C) × (1 mol O_2/4 mol e^{-1}) × (6.023 × 10^{23} molecules O_2/1 mol O_2) = 1.56 × 10^{15} O_2 s^{-1} cm^{-2} per mA cm^{-2}

In this work, # is 1.56 × 10^{15} s^{-1} cm^{-2} per mA cm^{-2}, and A is 0.04 cm^2, corresponding to the geometric area of the catalyst. The surface site density of all materials is reasonably approximated to be 10^{15} cm^{-2}. Therefore, N can be calculated using the formula $N = C_{dl}/C_s$ × 10^{15} cm^{-2}, where C_{dl} and C_s represent the double-layer and specific capacitance, respectively. For this calculation, a general C_s value of 0.035 mF cm^{-2} was used.

Table S9. Recently reported electrocatalyst activities for the OER in acidic media.

Electrocatalyst	**Overpotential (η_{10})**	**Tafel Slope (mV dec^{-1})**	**Ref.**
Ir/Fe_4N	316	61.5	15
Ir/Co_4N	319	66.9	15
Ir/Ni_4N	346	64	15
RuO_2/Co_3O_4-RuCo@NC	247	89	16
$Y_{1.85}Zn_{0.15}Ru_2O_{7-\delta}$	290	36.9	17
$Co_{0.05}Fe_{0.95}O_y$	650	110	18
$SrTi_{0.67}Ir_{0.33}O_3$	247	43	19
$Sr_{0.90}Na_{0.10}RuO_3$	170	40	20
IrCo alloy	270	71.8	21
Ru1-Pt_3Cu	220		22
$Ir_{0.2}Ni_{0.34}Co_{0.46}O_\delta$	280	40.4	23
np-$Ir_{70}Ni_{15}Co_{15}$	220	44.1	24
$Ta_{0.1}Tm_{0.1}Ir_{0.8}O_{2-\delta}$	226	64	25
$Ho_2Ru_2O_7$	280	36.86	26
Ru/MnO_2	161	29.4	27
IrO_2-Ta_2O_5	240	51.9	28
Pt-doped IrNi	308	45	29
$(Na_{0.33}Ce_{0.67})_2$-$Ir_{1-x}Ru_x)_2O_7$	190		30
HEA8	230	89.2	This work

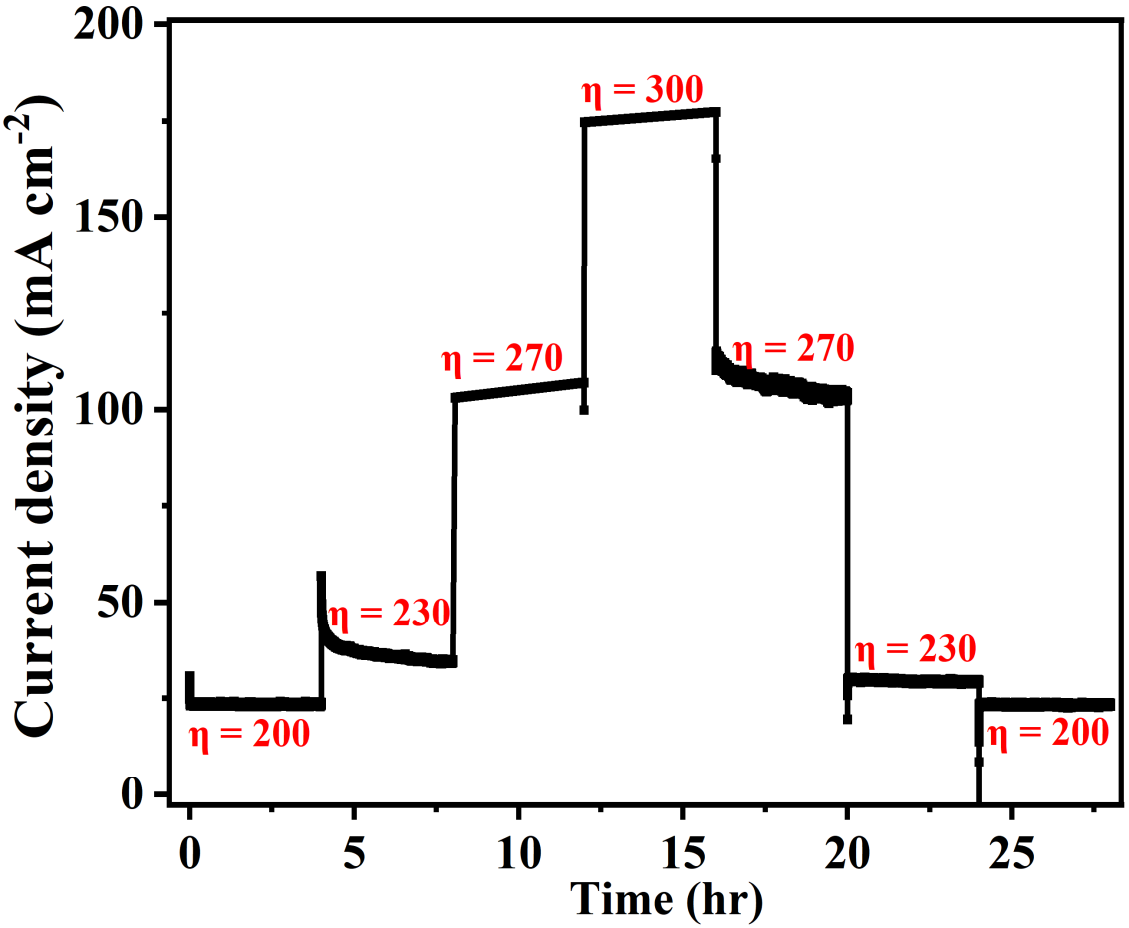

Figure S13. Chronoamperometry study of HEA8 at different potentials during the OER.

Table S10. Recently reported high-entropy alloy-based electrocatalysts for overall water splitting in acidic media.

Electrocatalyst	**Electrolyte**	**Potential @ geometric current density**	**Loading**	**Durability**	**Ref.**
RuIr-NC||RuIr-NC	0.05 M H_2SO_4	1.485 V @ 10 mA cm^{-2}	0.15 mg cm^{-2}	120 h @ 10 mA cm^{-2}	31
Co-RuIr||Co-RuIr	0.1 M $HClO_4$	1.52 V @ 10 mA cm^{-2}	-	25 h @ 10 mA cm^{-2}	32
Ru-Te nanorods|| Ru-Te nanorods	0.5 M H_2SO_4	1.52 V @ 10 mA cm^{-2}	-	24 h @ 5 mA cm^{-2}	33
ONPPGC/GC||ONPPGC/GC	0.5 M H_2SO_4	1.75 V @ 10 mA cm^{-2}	-	10 h @ 5 mA cm^{-2}	34
Ir-A@Fe@N CNT|| IrSA@Fe@N CNT	0.5 M H_2SO_4	1.51 V @ 10 mA cm^{-2}	0.00114 mg_{Ir} cm^{-2}	12 h @ 10 mA cm^{-2}	35
Co-MoS_2||Co-MoS_2	0.5 M H_2SO_4	1.90 V @ 10 mA cm^{-2}	-	-	36
IrO_2||M-$CoSe_{1.28}S_{0.72}$	0.5 M H_2SO_4	1.79 V @ 1 mA cm^{-2}	3 and 1 mg per cm^2 in anode and cathode	416 h @ 1 A cm^{-2}	12
IrO_2||$Ni_{96}W_4$/Cu	0.5 M H_2SO_4	1.88 V @ 1 mA cm^{-2}		-	37
Ir||Mo_3S_{13}-NCNT	0.5 M H_2SO_4	1.92 V @ 1 mA cm^{-2}	1.5 and 3 mg cm^{-2} in anode and cathode	1700 h @ 1.86 A cm^{-2}	38
IrO_2||$Cu_{44.4}Ni_{46}Mo_{9.6}$	0.5 M H_2SO_4	1.8 V @ 1 mA cm^{-2}	1.5 and 3 mg cm^{-2} in anode and cathode	48 h @ 1 A cm^{-2}	39
HEA8||HEA8	0.5 M H_2SO_4	1.51 V @ 10 mA cm^{-2}	0.25 mg cm^{-2}	30 h @ 55 mA cm^{-2}	This work

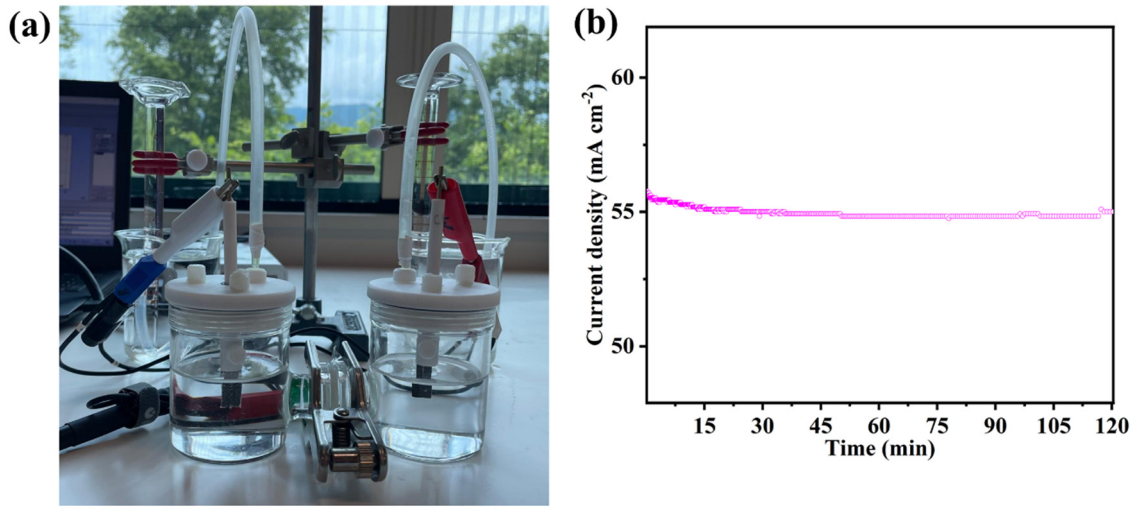

Figure S14. (a) Experimental setup for the Faradaic efficiency calculation of HEA8 for overall water splitting. (b) Chronoamperometric curve of HEA8||HEA8 obtained at 2 V.

Faradaic efficiency (FE) of overall water splitting catalyzed by HEA8

The FE of HEA8 in an acidic medium was calculated at an applied voltage of 2 V. The bifunctional electrocatalysts achieved a current density of 55 mA cm^{-2} at 2 V, with a geometric area of 0.18 cm^2 for the carbon cloth. The number of charges passed per second at the applied voltage equals (0.055 A × 0.18 cm^2 × 1 s) Coulombs, and the number of electrons passed per second equals (0.055 A × 0.18 cm^2 × 1 s)/96485 mol.

For the HER, since the transfer of two electrons is associated with the evolution of one H_2 molecule, the amount of H_2 produced per second due to the passage of electrons equals ((0.055 × 0.18 × 1)/(96485 × 2)) mol. At standard temperature and pressure, where the volume of 1 mol of gas is 22400 mL, the amount of H_2 produced per second is ((0.055 × 0.18 × 1 × 22400 mL)/(96485 × 2)) mL = 0.001149 mL.

For the OER, since the transfer of 4 electrons is associated with the evolution of one O_2 molecule, the amount of O_2 produced per second is ((0.055 × 0.18 × 1)/(96485 × 4)) mol. Thus, the volume of O_2 produced per second is ((0.055 × 0.18 × 1 × 22400 mL)/(96485 × 4)) mL = 0.00057459 mL.

Finally, the FE of the water splitting process was calculated using the following equation:

FE = (Amount of gas practically evolved × 100)/Theoretically calculated amount of gas

Table S11. FE calculation of HEA8.

Time (min)	O_2 gas evolution (mL)		FE (%)	H_2 gas evolution (mL)		FE (%)
	Theoretical	Experimental		Theoretical	Experimental	
20	0.7	0.708	98.80	1.5	1.51	99.30
40	1.5	1.52	98.68	2.8	3.02	93.02
60	2	2.21	95.23	4.2	4.29	97.90
80	2.7	2.72	92.59	5.5	5.59	98.92
100	3.5	3.53	96.41	6.5	6.98	93.12
120	4	4.23	95.20	8.7	8.79	97.81

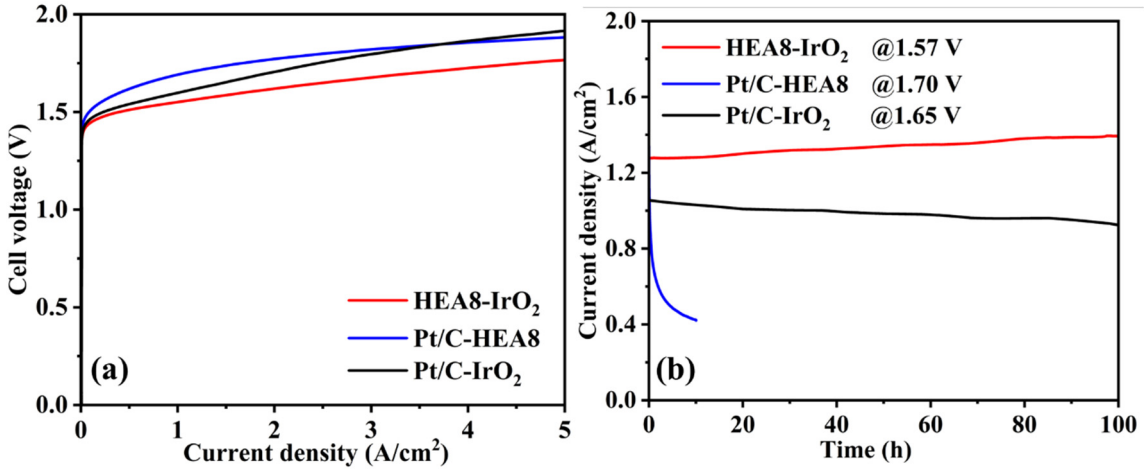

Figure S15. Performance of HEA8 in single-cell PEM water electrolyzer. (a) Current–density (*I–V*) polarization curves for HEA8||IrO_2, Pt/C||HEA8, and Pt/C||IrO_2 after cell activation. (b) Chronoamperometry curves of HEA8||IrO_2, Pt/C||HEA8, and Pt/C||IrO_2 at cell voltages of 1.57, 1.70, and 1.65 V, respectively.

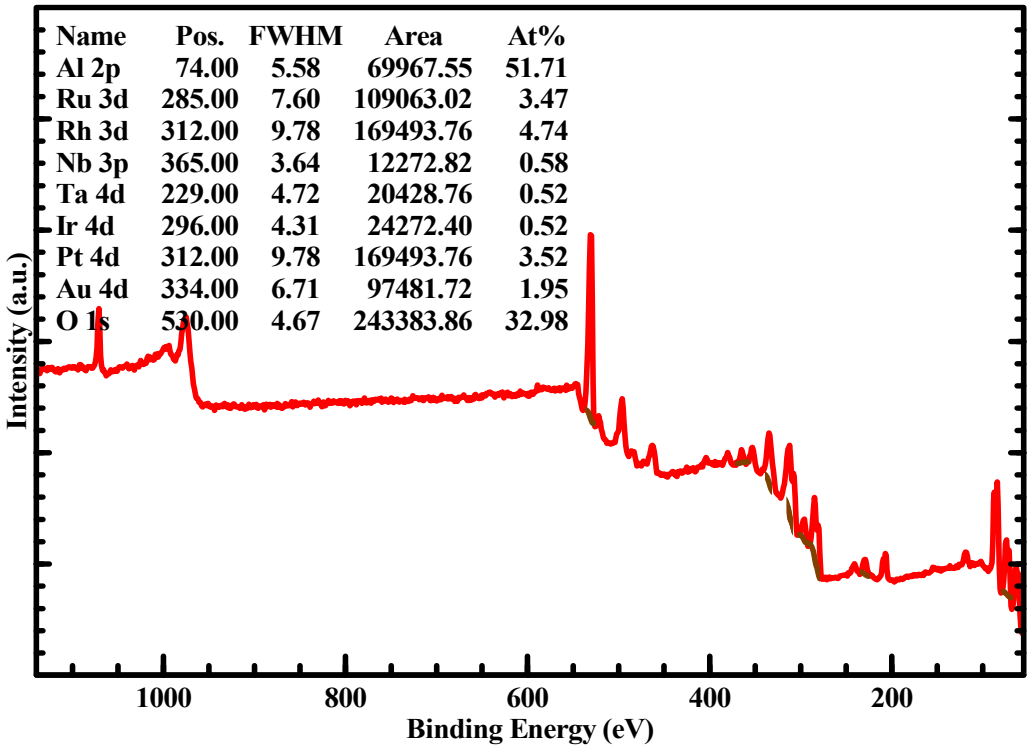

Figure S16. XPS survey spectrum of HEA8.

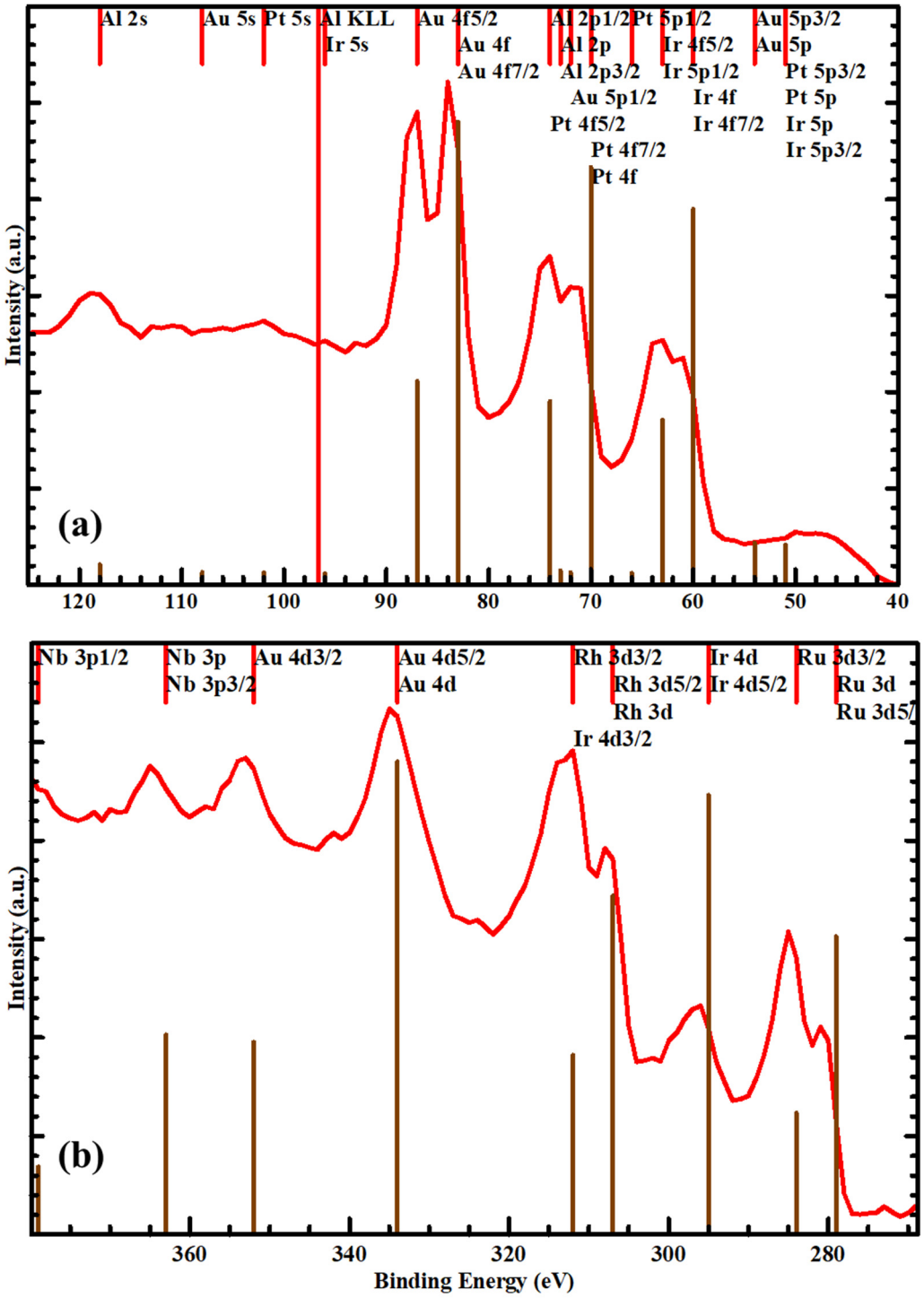

Figure S17. Core-level XPS spectra of HEA8 in the range of (a) 40–125 eV and (b) 270–380 eV, showing the 4f orbitals of Al, Ir, Pt, and Au, and the 3d orbitals of Ru, Rh, and Pt, respectively. The binding energies of each peak are shown in the figure.

References

1 I. S. Kwon, I. H. Kwak, G. M. Zewdie, S. J. Lee, J. Y. Kim, S. J. Yoo, J. G. Kim, J. Park and H. S. Kang, *Adv. Mater.*, 2022, **34**, e2205524.

2 I. H. Kwak, I. S. Kwon, G. M. Zewdie, T. T. Debela, S. J. Lee, J. Y. Kim, S. J. Yoo, J. G. Kim, J. Park and H. S. Kang, *ACS Nano*, 2022, **16**, 4278.

3 J. Deng, H. B. Li, J. P. Xiao, Y. C. Tu, D. H. Deng, H. X. Yang, H. F. Tian, J. Q. Li, P. J. Ren and X. H. Bao, *Energy Environ. Sci.*, 2015, **8**, 1594.

4 L. H. Zhang, L. L. Han, H. X. Liu, X. J. Liu and J. Luo, *Angew. Chem. Int. Ed.*, 2017, **56**, 13694.

5 N. C. Cheng, S. Stambula, D. Wang, M. N. Banis, J. Liu, A. Riese, B. W. Xiao, R. Y. Li, T. K. Sham, L. M. Liu, G. A. Botton and X. L. Sun, *Nat. Commun.*, 2016, **7**, 13638.

6 J. Q. Zhang, Y. F. Zhao, X. Guo, C. Chen, C. L. Dong, R. S. Liu, C. P. Han, Y. D. Li, Y. Gogotsi and G. X. Wang, *Nat. Catal.*, 2018, **1**, 985.

7 K. Jiang, B. Y. Liu, M. Luo, S. C. Ning, M. Peng, Y. Zhao, Y. R. Lu, T. S. Chan, F. M. F. de Groot and Y. W. Tan, *Nat. Commun.*, 2019, **10**, 1743.

8 Z. Jia, K. Nomoto, Q. Wang, C. Kong, L. G. Sun, L. C. Zhang, S. X. Liang, J. Lu and J. J. Kruzic, *Adv. Funct. Mater.*, 2021, **31**, 2101586.

9 H. Y. Jin, S. Sultan, M. R. Ha, J. N. Tiwari, M. G. Kim and K. S. Kim, *Adv. Funct. Mater.*, 2020, **30**, 2000531.

10 H. H. Wei, K. Huang, D. Wang, R. Y. Zhang, B. H. Ge, J. Y. Ma, B. Wen, S. Zhang, Q. Y. Li, M. Lei, C. Zhang, J. Irawan, L. M. Liu and H. Wu, *Nat. Commun.*, 2017, **8**, 1490.

11 Y. C. Yao, X. K. Gu, D. S. He, Z. J. Li, W. Liu, Q. Xu, T. Yao, Y. Lin, H. J. Wang, C. M. Zhao, X. Q. Wang, P. Q. Yin, H. Li, X. Hong, S. Q. Wei, W. X. Li, Y. D. Li and Y. Wu, *J. Am. Chem. Soc.*, 2019, **141**, 19964.

12 X.-L. Zhang, P.-C. Yu, X.-Z. Su, S.-J. Hu, L. Shi, Y.-H. Wang, P.-P. Yang, F.-Y. Gao, Z.-Z. Wu, L.-P. Chi, Y.-R. Zheng and M.-R. Gao, *Sci. Adv.*, 2023, **9**, eadh2885.

13 J. D. Benck, Z. Chen, L. Y. Kuritzky, A. J. Forman and T. F. Jaramillo, *ACS Catal.*, 2012, **2**, 1916.

14 Z. W. Chen, J. Li, P. Ou, J. E. Huang, Z. Wen, L. X. Chen, X. Yao, G. Cai, C. C. Yang, C. V. Singh and Q. Jiang, *Nat. Commun.*, 2024, **15**, 359.

15 B. M. Tackett, W. Sheng, S. Kattel, S. Yao, B. Yan, K. A. Kuttiyiel, Q. Wu and J. G. Chen, *ACS Catal.*, 2018, **8**, 2615.

16 Z. Fan, J. Jiang, L. Ai, Z. Shao and S. Liu, *ACS Appl. Mater. Interfaces*, 2019, **11**, 47894.

17 Q. Feng, Q. Wang, Z. Zhang, Y. Xiong, H. Li, Y. Yao, X.-Z. Yuan, M. C. Williams, M. Gu, H. Chen, H. Li and H. Wang, *Appl. Catal. B*, 2019, **244**, 494.

18 W. L. Kwong, C. C. Lee, A. Shchukarev and J. Messinger, *Chem. Commun.*, 2019, **55**, 5017.

19 X. Liang, L. Shi, Y. Liu, H. Chen, R. Si, W. Yan, Q. Zhang, G.-D. Li, L. Yang and X. Zou, *Angew. Chem. Int. Ed.*, 2019, **58**, 7631.
20 M. Retuerto, L. Pascual, F. Calle-Vallejo, P. Ferrer, D. Gianolio, A. G. Pereira, Á. García, J. Torrero, M. T. Fernández-Díaz, P. Bencok, M. A. Peña, J. L. G. Fierro and S. Rojas, *Nat. Commun.*, 2019, **10**, 2041.
21 X. Sun, F. Liu, X. Chen, C. Li, J. Yu and M. Pan, *Electrochim. Acta*, 2019, **307**, 206.
22 Y. Yao, S. Hu, W. Chen, Z.-Q. Huang, W. Wei, T. Yao, R. Liu, K. Zang, X. Wang, G. Wu, W. Yuan, T. Yuan, B. Zhu, W. Liu, Z. Li, D. He, Z. Xue, Y. Wang, X. Zheng, J. Dong, C.-R. Chang, Y. Chen, X. Hong, J. Luo, S. Wei, W.-X. Li, P. Strasser, Y. Wu and Y. Li, *Nat. Catal.*, 2019, **2**, 304.
23 W. Q. Zaman, W. Sun, M. Tariq, Z. Zhou, U. Farooq, Z. Abbas, L. Cao and J. Yang, *Appl. Catal. B*, 2019, **244**, 295.
24 Y. Zhao, M. Luo, S. Chu, M. Peng, B. Liu, Q. Wu, P. Liu, F. M. F. de Groot and Y. Tan, *Nano Energy*, 2019, **59**, 146.
25 S. Hao, H. Sheng, M. Liu, J. Huang, G. Zheng, F. Zhang, X. Liu, Z. Su, J. Hu, Y. Qian, L. Zhou, Y. He, B. Song, L. Lei, X. Zhang and S. Jin, *Nat. Nanotechnol.*, 2021, **16**, 1371.
26 J. Yan, J. Zhu, D. Chen, S. Liu, X. Zhang, S. Yu, Z. Zeng, L. Jiang and F. Du, *J. Mater. Chem. A*, 2022, **10**, 9419.
27 C. Lin, J.-L. Li, X. Li, S. Yang, W. Luo, Y. Zhang, S.-H. Kim, D.-H. Kim, S. S. Shinde, Y.-F. Li, Z.-P. Liu, Z. Jiang and J.-H. Lee, *Nat. Catal.*, 2021, **4**, 1012.
28 Y. Furusho and F. Amano, *Electrochemistry*, 2021, **89**, 234.
29 J. S. Choi, A. S. T. Smith, N. P. Williams, T. Matsubara, M. Choi, J. W. Kim, H. J. Kim, S. Choi and D. H. Kim, *Adv. Funct. Mater.*, 2020, **30**, 2003935.
30 K. Sardar, E. Petrucco, C. I. Hiley, J. D. B. Sharman, P. P. Wells, A. E. Russell, R. J. Kashtiban, J. Sloan and R. I. Walton, *Angew. Chem. Int. Ed.*, 2014, **53**, 10960.
31 D. Wu, K. Kusada, S. Yoshioka, T. Yamamoto, T. Toriyama, S. Matsumura, Y. Chen, O. Seo, J. Kim, C. Song, S. Hiroi, O. Sakata, T. Ina, S. Kawaguchi, Y. Kubota, H. Kobayashi and H. Kitagawa, *Nat. Commun.*, 2021, **12**, 1145.
32 J. Shan, T. Ling, K. Davey, Y. Zheng and S. Z. Qiao, *Adv. Mater.*, 2019, **31**, 1900510.
33 J. Wang, L. Han, B. Huang, Q. Shao, H. L. Xin and X. Huang, *Nat. Commun.*, 2019, **10**, 5692.
34 S. L. J. Lai, F. Wu, M. Saqib, R. Luque and G. Xu, *Energy Environ. Sci.*, 2016, **9**, 1210.
35 F. Luo, H. Hu, X. Zhao, Z. Yang, Q. Zhang, J. Xu, T. Kaneko, Y. Yoshida, C. Zhu and W. Cai, *Nano Lett.*, 2020, **20**, 2120.
36 Q. Xiong, X. Zhang, H. Wang, G. Liu, G. Wang, H. Zhang and H. Zhao, *Chem. Commun.*, 2018, **54**, 3859.
37 H. Kim, H. Park, D. K. Kim, S. H. Oh, I. Choi and S. K. Kim, *ACS Sustainable Chem. Eng.*, 2019, **7**, 8265.

38 P. K. R. Holzapfel, M. Bühler, D. Escalera-López, M. Bierling, F. D. Speck, K. J. J. Mayrhofer, S. Cherevko, C. V. Pham and S. Thiele, *Small*, 2020, **16**, 2003161.
39 K. J. Choi, H. Kim and S.-K. Kim, *J. Power Sources*, 2021, **506**, 230200.